Applied Physics Letters

Electric double layers allow for opaque electrodes in high performance organic optoelectronic devices

Cite as: Appl. Phys. Lett. **101**, 173302 (2012); https://doi.org/10.1063/1.4762823
Submitted: 30 August 2012 . Accepted: 08 October 2012 . Published Online: 22 October 2012

Bo Li, Simon Dalgleish, Yasuhito Miyoshi, Hirofumi Yoshikawa, Michio M. Matsushita, and Kunio Awaga

Electric double layers allow for opaque electrodes in high performance organic optoelectronic devices

Bo Li,[1,2,a)] Simon Dalgleish,[1] Yasuhito Miyoshi,[1] Hirofumi Yoshikawa,[1] Michio M. Matsushita,[1] and Kunio Awaga[1,3,b)]
[1]*Department of Chemistry and Research Center for Materials Science, Nagoya University, Nagoya 464-8602, Japan*
[2]*Department of Applied Physics, Zhejiang University of Technology, Hangzhou 310023, People's Republic of China*
[3]*CREST, JST, Nagoya 464-8602, Japan*

(Received 30 August 2012; accepted 8 October 2012; published online 22 October 2012)

We report that opaque electrodes can be used for high-performance organic optoelectronic devices, facilitated by the electric double layers (EDLs) formed in ionic liquids. For the photocell, gold/poly(3-hexylthiophene-2,5-diyl) (P3HT):[6,6]-phenyl C_{61} butyric acid methyl ester (PCBM)/ionic liquid/silver, the EDLs enable a large photocurrent response, without the electrodes being superimposed. The external quantum efficiency and responsivity can reach 61.2% and 272 mA/W, respectively. The specific detectivity can reach 1.9×10^{13} Jones, which is larger than silicon-based detectors. This type of architecture will renew the operation principle and material choice for organic photocells, because transparency is no longer an indispensable condition for the electrodes.
 [http://dx.doi.org/10.1063/1.4762823]

To date, all organic photocells, such as organic photodetectors (OPDs) and organic solar cells (OSCs),[1] which can be operated under passive conditions suffer a common structural drawback; at least one of the electrodes must be transparent, because the incident light must be able to pass through them to efficiently excite the photoactive layer.[2] This limitation is caused by the poor mobilities of organic semiconductors, which limits the active area for photo-conversion to the region of electrode superposition. However, the choice of transparent electrode materials is severely limited. Among them, indium tin oxide (ITO) is the most popular choice because of its high conductivity, transparency,[3] and commercial available, but it is expensive and brittle.[4] In recent years, conducting polymers[5] and graphene[6] have been proposed as replacements for ITO as a transparent electrode. However, for conducting polymers, their thermal and chemical stability under operating conditions remains a concern,[7] and for graphene, its poor hydrophilicity has been shown to substantially decrease the performance of solution-processed devices,[8] and its preparation method is complicated.[9] The requirement of both transparency and conductivity for electrode materials, therefore, poses a significant challenge to the development of organic photocells. Put another way, if transparency were no longer an essential condition for electrode choice, any conductor could be used, with properties better tailored to their application.

To realize opaque electrode based high-performance organic optoelectronic conversion, the present work is based on the idea of combining displacement current and the electric double layers (EDLs) in ionic liquids, which have attracted much attention in electronics, due to their potential applications in various devices, such as capacitors, batteries, solar cells, fuel cells, and actuators.[10] According to the Helmholtz model,[11] an EDL can be formed at an ionic liquid/solid interface,[12] and the potential drop at the interface is confined within the outer Helmholtz plane (OHP). The ultrathin potential drop region, caused by the EDL, allows for high density charge accumulation,[13] which has been exploited for organic thin film transistors (OTFTs).[14] Displacement current is not an electric current of moving charges, but a time-varying change in the electric field, to which the dielectric polarization in materials makes a dominant contribution. When the EDLs have been introduced into the photocells, the present mechanism is not suitable for solar cells which produce steady-state current, but it is suitable for organic photodetection, sensing, and optical communication.

The opaque electrode based organic photocells, with the device structures of metal (gold (Au), copper (Cu), aluminum (Al))/active layer/ionic liquid/silver (Ag), were fabricated, in which the ionic liquid *N*,*N*-diethyl-*N*-methyl(2-methoxyethyl) ammonium bis(trifluoromethylsulfonyl)-imide (DEME-TFSI) was used, with its layer fabricated by drop casting (thickness $d = 0.15$ mm). The active layer was a bulk heterojunction (BHJ) composite of poly(3-hexylthiophene-2,5-diyl) (P3HT) and [6,6]-phenyl C_{61} butyric acid methyl ester (PCBM) (1:1 weight-ratio) ($d = 170$ nm) fabricated by spin coating. Films of Au, Cu, Al, and Ag ($d = 200$ nm) were used as the opaque electrodes, and were fabricated by vacuum vapor deposition. The structure of the photocells is schematically shown in Figure 1(a), and the measurement setup is illustrated in Figure S1.[15] The photocell was irradiated from the Ag side by a 532 nm continuous wave (CW) laser with an output power density of 5 mW/cm^2, modulated by a light chopper at 3000 Hz, under a zero bias voltage. Since the maximum transmittance of the 200 nm thick Ag film is about 0.24% in the range of 400 to 800 nm (see Figure S3[15]), the P3HT:PCBM active layer was irradiated in the

a)Electronic mail: libo@zjut.edu.cn.
b)Electronic mail: awaga@mbox.chem.nagoya-u.ac.jp.

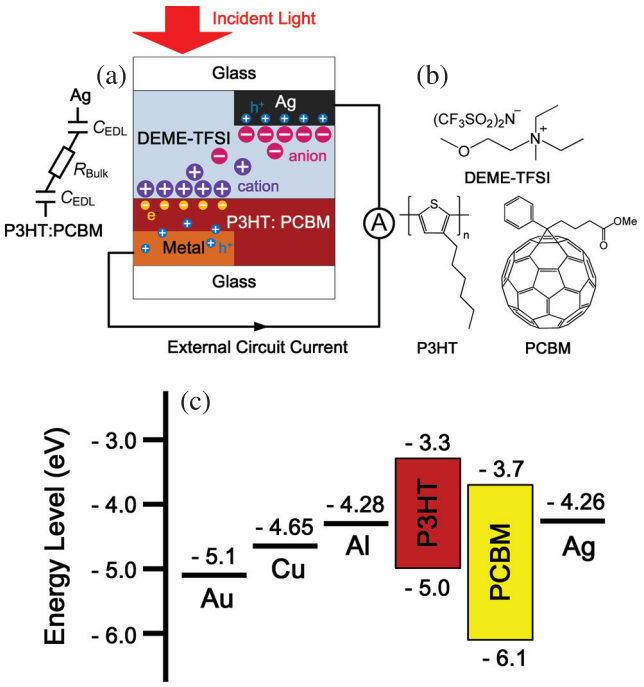

FIG. 1. (a) The device structure of metal (Au, Cu, Al)/P3HT:PCBM/DEME-TFSI/Ag. The equivalent circuit is also shown, in which the two C_{EDL} are the capacitors formed at the interfaces, and the R_{Bulk} is the resistor of bulk DEME-TFSI. (b) The molecular structures of P3HT, PCBM, and DEME-TFSI. (c) Energy level diagram of the components in the devices.

non-superimposed area between the Ag cathode and the anode (Au, Cu, Al) electrodes, as described in Figure 1(a). The photocurrent was measured using a current amplifier and an oscilloscope.

The red curve in Figure 2 shows the time dependence of the incident light power density, measured using a silicon photodiode. The time trajectory of the photocurrent for the metal/P3HT:PCBM/DEME-TFSI/Ag photocells is shown in Figure 2, in which the black, green, and blue curves represents the anode metals Au, Cu, and Al, respectively. The Au/P3HT:PCBM/DEME-TFSI/Ag photocell yielded the largest photocurrent response, compared to the other two photocells. When the light turns on, the photocurrent quickly

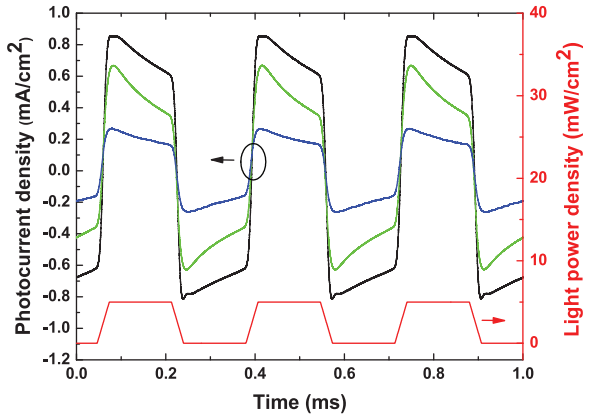

FIG. 2. The photoresponse of Metal (Au, Cu, Al)/P3HT:PCBM/ DEME-TFSI/Ag (black is Au, green is Cu, and blue is Al) photocells under illumination of a light-chopper-modulated 532 nm laser (3000 Hz) with a power density of 5 mW/cm^2. The red curve shows the time dependence of the incident light power density.

increases, and, after making a maximum, it shows a gradual decrease. When the light turns off, the current suddenly changes the polarization from positive to negative, and, after passing through a negative peak, it shows a gradual decrease. The energy level diagram is shown in Figure 1(c), and depicts the highest occupied molecular orbital (HOMO) energies, the lowest unoccupied molecular orbital (LUMO) energies, and the work functions of the individual component materials. The order of efficiencies can be rationalized simply by consideration of the work functions of the anode metals. Since the cathode is constant for each device, a larger built-in voltage is expected for higher work function anode metals, leading to more efficient charge separation in the device; thus, Au is larger than Cu, which, in turn is larger than Al. However, the energy level diagram also illustrates another important point. The work function of Au is larger than the HOMO level of P3HT, therefore, it is unnecessary to introduce any interfacial layer between the active layer and the anode to improve the efficiency of hole collection,[16] which is beneficial to produce a large photocurrent. Such an interfacial layer is commonplace in the case of ITO based devices, usually in the form of poly(3,4-ethylenedioxythiophene)/poly(styrenesulfonate) (PEDOT:PSS), to reduce the energy barrier to hole collection.[17] The work functions of Cu and Al are both smaller than the HOMO level of P3HT, which will produce a built-in electric field at the metal/organic interface, which prevents holes injecting into the corresponding metal electrodes. One merit of such a device architecture is therefore to provide many more choices for the electrode materials, which can better match the energy levels of the organic semiconductors.

Because the active layer was spin-cast on the top of the anode metal, the morphology of the metal film is very important for the efficiency of photocurrent collection. The topography images of the Au, Cu, and Al films (see Figures S4, S5, and S6[15]) indicate a large number of nanostructures, with a diameter and height of about 20 nm in both the Au and Cu films, but a much smoother film for Al. The surface area of the Au, Cu, and Al films increases by 26%, 27%, and 8%, respectively, compared to an idealized flat surface. The increased contact area between metal electrode and active layer will lead to greater efficiency of charge collection at the metal-polymer interface. The nanostructuring of the metal surface allows for electrode penetration into the active layer, and effectively reduces the charge-transport distance, improving photocurrent collection. The topography of the Au and Cu films is similar, but the Au based photocell can produce a larger photocurrent than the Cu based cell, due to their work function difference, discussed previously.

Figure 1(a) includes the equivalent circuit of the Metal/P3HT:PCBM/DEME-TFSI/Ag photocells, in which there are two capacitors and one resistor describing the ionic liquid, due to the formation of EDLs at both the solid/liquid interfaces. The modulated periodical light-on generates excitons in the P3HT:PCBM active layer. After dissociation of the excitons to form mobile charge carriers, the holes are collected by the metal anode and electrons are accumulated at P3HT:PCBM/DEME-TFSI interface, which induces the formation of an EDL. The formation of an EDL at the P3HT:PCBM/DEME-TFSI interface, in turn, induces the

formation of an EDL at the DEME-TFSI/Ag interface, which is facilitated by the high ionic conductivity of the ionic liquid.[18] The formation of an EDL at the DEME-TFSI/Ag interface will draw the holes from the metal electrode to the Ag electrode, which generates the external circuit current described in Figure 1(a). During the light-on period, the EDLs are charged up, and, in the following light-off period, the negative transient photocurrent appears due to the discharging of the EDLs.

The external quantum efficiency (EQE) was estimated for the Au/P3HT:PCBM/ DEME-TFSI/Ag photocell. Figure 3(a) shows the wavelength dependence of the EQE, which was calculated from the peak values of the transient photocurrent during the light-on period. High EQE values were observed, suggesting that the photon-electron conversion process is rather efficient under the present mechanism. The shape of the EQE curve is similar to the corresponding absorption spectrum of the P3HT:PCBM blend film (see Figure 3(b)). The peak value of the EQE reaches 61.2% at 495 nm, which is similar to conventional P3HT:PCBM based OSCs, which use ITO as the transparent electrode material.[19]

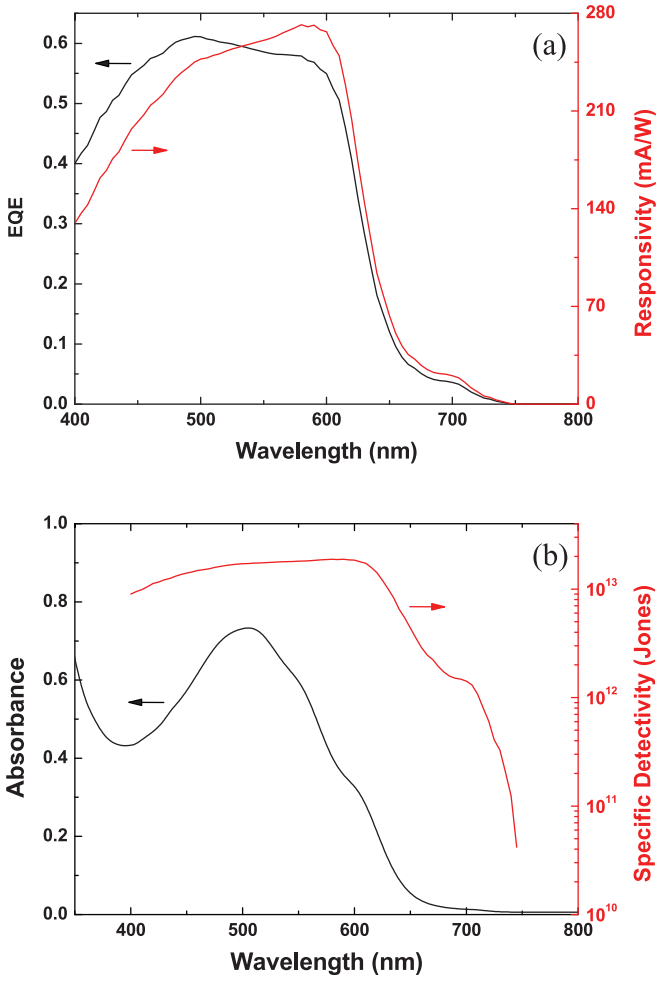

FIG. 3. (a) EQE (black line) and responsivity (red line) spectra of the Au/P3HT:PCBM/DEME-TFSI/Ag photocell obtained by irradiation with light-chopper-modulated monochromatic light from 400 nm to 800 nm (3000 Hz) without a bias voltage. (b) Specific detectivity spectrum (red), which is calculated from the responsivity and the absorption spectrum (black) of the P3HT:PCBM (1:1, by weight) blend film.

Furthermore, the responsivity R_i of this photocell was calculated, using Eq. (1)

$$R_{\mathrm{i}} = \frac{I_{\mathrm{ph}}}{P_{\mathrm{opt}}} = \frac{q \cdot \lambda \cdot EQE}{h \cdot c}, \tag{1}$$

where I_{ph} is the produced photocurrent, P_{opt} is the input light power, hc/λ is the photon energy, and q denotes the elementary charge. The responsivity at 580 nm, without a bias voltage, corresponds to 272 mA/W, which is much larger than that of conventional organic photodetectors operated by a bias voltage,[20] and is close to the commercially available silicon photodiodes.

As mentioned previously, the present photocell is suitable as a OPD, whose figure of merit is the noise equivalent power (NEP), i.e., the minimum impinging optical power that a detector can distinguish from the background noise, which can be calculated by Eq. (2)

$$NEP = (A\Delta f)^{1/2}/D^*, \tag{2}$$

where A is the effective area of the photodetector in cm^2, Δf is the electrical bandwidth in Hz, and D^* is the specific detectivity measured in units of Jones. If the dark current is the major contribution to the noise, then D^* can be expressed[21] as

$$D^* = R_i/(2qJ_d)^{1/2}, \tag{3}$$

where R_i is the responsivity, q is the elementary charge, and J_d is the dark current. The D^* at zero bias is shown in Figure 3(b), which was calculated based on the derived responsivity and measured dark current. At 580 nm, $D^* = 1.9 \times 10^{13}$ Jones, which is higher than that of silicon based detectors (about 8×10^{12} Jones) in the visible range. A NEP of 1.2×10^{-14} W/Hz$^{1/2}$ at 580 nm was calculated based on Eq. (2), which is similar to the silicon based detectors (about 1.3×10^{-14} W/Hz$^{1/2}$). From the equivalent circuit of the present photocell described in Figure 1(a), two built-in EDL capacitors are shown, which can effectively decrease the dark current, and, as a result, a high specific detectivity and low NEP can be obtained.

In order to understand the influence of the introduced EDLs in the present photocell on the ultra-fast and high-speed photoresponse features, a nanosecond pulsed laser with a wavelength of 532 nm, and a light-emitting diode (LED) with the central wavelength of 525 nm switched on and off by a function generator, were used to determine the photoresponse of the photocell, respectively. The impulse response of the photocell is shown in Figure 4(a), which was recorded by the photocell directly connected to a 1 GHz bandwidth oscilloscope, with an input resistance of 50 Ω. Under zero bias, the rise time (10%-90%) and fall time (90%-10%) and the full width at half maximum (FWHM) of the photocell are 2.1 ns, 147.6 ns, and 29.9 ns, respectively, in which the fall time and FWHM are much smaller than the conventional P3HT:PCBM based OPDs.[22] From the fast Fourier transformation (FFT) of the impulse response (see Figure 4(b)), a −3 dB cutoff frequency of about 2.6 MHz can be derived. This would suggest that at zero bias, the

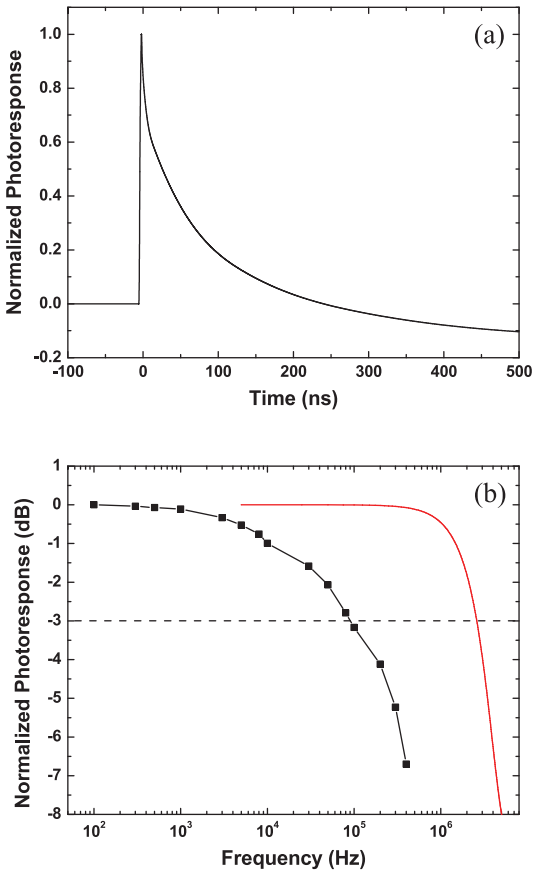

FIG. 4. (a) Impulse response of the Au/P3HT:PCBM/DEME-TFSI/Ag photocell under a zero bias voltage following a 1 ns laser pulse ($\lambda = 532$ nm; beam diameter of 0.26 mm; pulse energy of 5 μJ). (b) Frequency response of the Au/P3HT:PCBM/DEME-TFSI/Ag photocell under a zero bias voltage following a modulated LED (central $\lambda = 525$ nm; light spot diameter of 2 mm; LED power density of 3 mW/cm^2) (black curve), and fast Fourier transformation of the impulse response (red curve).

present photocell is more suitable for ultra-fast photodetection, compared to a conventional architecture, since it benefits from the introduced EDLs in series, decreasing the device capacitance. However, the negative photoresponse polarization observed in Figure 4(a) indicates that a recovery period is needed for the device, due to the discharge process of the EDLs, which will decrease the high-speed photoresponse of the present photocell, as calculated from the decay profile. The experimentally determined frequency-dependent photoresponse of the present photocell is shown in Figure 4(b), where the normalized photoresponse is plotted versus the modulated LED frequency, varied from 100 Hz to 400 kHz. Under the same zero bias conditions, the −3 dB cutoff frequency of the present photocell is about 90 KHz (shown in Figure 4(b)) which is just a little lower than the conventional P3HT:PCBM based OPDs (about 100 kHz)[23] irradiated by LED or laser diode, but much lower than the calculated −3 dB cutoff. One reason for this may be that the specific capacitance of the EDLs induced in DEME-TFSI diminishes at frequencies above ~100 kHz,[24] which is close to the observed frequency cutoff for the device. Additionally, the effective device area is much smaller when irradiated by the pulsed laser than by the LED, which substantially decreases the effective device capacitance during operation, so the −3 dB cutoff frequency derived from FFT of the impulse response would overestimate the cutoff frequency, compared to measurement by the LED.

It can be concluded that opaque electrodes can be used to realize high-efficiency and high-detectivity organic optoelectronic devices, when combined with EDLs formed in ionic liquids, as high density charge accumulation can occur at the solid/liquid interfaces, leading to enhanced charge separation. The EQE and responsivity of this photocell can reach 61.2% and 272 mA/W, respectively. Because the EDLs effectively decrease the dark current, the specific detectivity of this photocell can reach 1.9×10^{13} Jones, which is comparably larger than silicon based detectors in the visible region. We hope that such opaque electrode based optoelectronic conversion will renew the operation principle, the photocell design, and lead to material innovation for organic photodetectors, sensors and optical communication devices, because transparency is no longer an indispensable condition for the electrodes.

This research was supported by a Grant-in-Aid for Scientific Research from the Ministry of Education, Culture, Sports, Science, and Technology (MEXT) of Japan. Dr. Li thanks the National Science Foundation of China (No. 61008008).

[1]X. Gong, M. Tong, Y. Xia, W. Cai, J. S. Moon, Y. Cao, G. Yu, C. L. Shieh, B. Nilsson, and A. J. Heeger, Science **325**, 1665 (2009); J. Y. Kim, K. Lee, N. E. Coates, D. Moses, T. Q. Nguyen, M. Dante, and A. J. Heeger, *ibid*. **317**, 222 (2007); P. Peumans, S. Uchida, and S. R. Forrest, Nature **425**, 158 (2003).
[2]S. Günes, H. Neugebauer, and N. S. Sariciftci, Chem. Rev. **107**, 1324 (2007); K. M. Coakley and M. D. McGehee, Chem. Mater. **16**, 4533 (2004).
[3]C. G. Granqvist and A. Hultåker, Thin Solid Films **411**, 1 (2002).
[4]M. Helgesen, R. Søndergaard, and F. C. Krebs, J. Mater. Chem. **20**, 36 (2010); Y. H. Kim, C. Sachse, M. L. Machala, C. May, L. Müller-Meskamp, and K. Leo, Adv. Funct. Mater. **21**, 1076 (2011).
[5]S. I. Na, S. S. Kim, J. Jo, and D. Y. Kim, Adv. Mater. **20**, 4061 (2008); Y. Zhou, H. Cheun, S. Choi, W. J. Potscavage, C. Fuentes-Hernandez, and B. Kippelen, Appl. Phys. Lett. **97**, 153304 (2010).
[6]L. G. D. Acro, Y. Zhang, C. W. Schlenker, K. Ryu, M. E. Thompson, and C. Zhou, ACS Nano **4**, 2865 (2010); G. Jo, S. I. Na, S. H. Oh, S. Lee, T. S. Kim, G. Wang, M. Choe, W. Park, J. Yoon, D. Y. Kim, Y. H. Kahng, and T. Lee, Appl. Phys. Lett. **97**, 213301 (2010).
[7]H. E. Yin, C. F. Lee, and W. Y. Chiu, Polymer **52**, 5065 (2011).
[8]Y. Wang, X. Chen, Y. Zhong, F. Zhu, and K. P. Loh, Appl. Phys. Lett. **95**, 063302 (2009).
[9]F. Bonaccorso, Z. Sun, and A. C. Ferrari, Nat. Photonics **4**, 611 (2010).
[10]D. Kuang, P. Wang, S. Ito, S. M. Zakeeruddin, and M. Grätzel, J. Am. Chem. Soc. **128**, 7732 (2006); W. Lu, A. G. Fadeev, B. Qi, E. Smela, B. R. Mattes, J. Ding, G. M. Spinks, J. Mazurkiewicz, D. Zhou, G. G. Wallace, D. R. MacFarlane, S. A. Forsyth, and M. Forsyth, Science **297**, 983 (2002); S. Seki, Y. Kobayashi, H. Miyashiro, Y. Ohno, A. Usami, Y. Mita, N. Kihira, M. Watanabe, and N. Terada, J. Phys. Chem. B **110**, 10228 (2006); C. Arbizzani, M. Biso, D. Cericola, M. Lazzari, F. Soavi, and M. Mastragostino, J. Power Sources **185**, 1575 (2008).
[11]H. von Helmholtz, Ann. Phys. Chem. **7**, 337 (1879); H. Wang and L. Pilon, J. Phys. Chem. C **115**, 16711 (2011).
[12]B. Li, Y. Noda, L. Hu, H. Yoshikawa, M. M. Matsushita, and K. Awaga, Appl. Phys. Lett. **100**, 163304 (2012).
[13]H. Yuan, H. Shimotani, A. Tsukazaki, A. Ohtomo, M. Kawasaki, and Y. Iwasa, Adv. Funct. Mater. **19**, 1046 (2009).
[14]Y. Xia, J. H. Cho, J. Lee, P. P. Ruden, and C. D. Frisbie, Adv. Mater. **21**, 2174 (2009).
[15]See supplementary material at http://dx.doi.org/10.1063/1.4762823 for device fabrication, characterization, experimental setup, and surface morphology.
[16]M. D. Irwin, D. B. Buchholz, A. W. Hains, R. P. H. Chang, and T. J. Marks, Proc. Natl. Acad. Sci. U.S.A. **105**, 2783 (2008); V. Shrotriya, G. Li, Y. Yao, C. W. Chu, and Y. Yang, Appl. Phys. Lett. **88**, 073508 (2006);

Y. Sun, C. J. Takacs, S. R. Cowan, J. H. Seo, X. Gong, A. Roy, and A. J. Heeger, Adv. Mater. **23**, 2226 (2011).
[17]C. J. Ko, Y. K. Lin, F. C. Chen, and C. W. Chu, Appl. Phys. Lett. **90**, 063509 (2007).
[18]R. Misra, M. McCarthy, and A. F. Hebard, Appl. Phys. Lett. **90**, 052905 (2007).
[19]G. Zhao, Y. He, and Y. Li, Adv. Mater. **22**, 4355 (2010); M. Campoy-Quiles, T. Ferenczi, T. Agostinelli, P. G. Etchegoin, Y. Kim, T. D. Anthopoulos, P. N. Stavrinou, D. D. C. Bradley, and J. Nelson, Nature Mater. **7**, 158 (2008); H. Zhang and J. Ouyang, Org. Electron. **12**, 1864 (2011).
[20]A. Iwasaki, L. Hu, R. Suizu, K. Nomura, H. Yoshikawa, K. Awaga, Y. Noda, K. Kanai, Y. Ouchi, K. Seki, and H. Ito, Angew. Chem., Int. Ed. **48**, 4022 (2009); G. Zhang, W. Li, B. Chu, Z. Su, D. Yang, F. Yan, Y. Chen, D. Zhang, L. Han, J. Wang, H. Liu, G. Che, Z. Zhang, and Z. Hu, Org. Electron. **10**, 352 (2009); K. S. Narayan and T. B. Singh, Appl. Phys. Lett. **74**, 3456 (1999); G. A. O'Brien, A. J. Quinn, D. A. Tanner, and G. A. Redmond, Adv. Mater. **18**, 2379 (2006).
[21]A. R. Jha, *Infrared Technology-Applications to Electro-Optics, Photonic Devices, and Sensors* (John Wiley & Sons, New York, 2000), p. 245; P. Bhattacharya, *Semiconductor Optoelectronics Device* (Prentice-Hall, Upper Saddle River, NJ, 1997), p. 345.
[22]S. Züfle, N. Christ, S. W. Kettlitz, S. Valouch, and U. Lemmer, Appl. Phys. Lett. **97**, 063306 (2010); M. Punke, S. Valouch, S. W. Kettlitz, N. Christ, C. Gärtner, M. Gerken, and U. Lemmer, *ibid.* **91**, 071118 (2007).
[23]W. W. Tsai, Y. C. Chao, E. C. Chen, H. W. Zan, H. F. Meng, and C. S. Hsu, Appl. Phys. Lett. **95**, 213308 (2009); L. Salamandra, G. Susanna, S. Penna, F. Brunetti, and A. Reale, IEEE Photonics Technol. Lett. **23**, 780 (2011).
[24]H. Yuan, H. Shimotani, J. Ye, S. Yoon, H. Aliah, A. Tsukazaki, M. Kawasaki, and Y. Iwasa, J. Am. Chem. Soc. **132**, 18402 (2010).